

# JOINT SPARSITY-DRIVEN INVERSION AND MODEL ERROR CORRECTION FOR RADAR IMAGING

*N. Özben Önhon and Müjdat Çetin*

Faculty of Engineering and Natural Sciences, Sabancı University, Orhanlı, Tuzla, 34956 Istanbul, Turkey

## ABSTRACT

Solution of inverse problems in imaging requires the use of a mathematical model of the observation process. However such models often involve errors and uncertainties themselves. The application of interest in this paper is synthetic aperture radar (SAR) imaging, which particularly suffers from motion-induced model errors. These types of errors result in phase errors in SAR data which cause defocusing of the reconstructed image. Mostly, phase errors vary only in cross-range direction. However, in many situations, it is possible to encounter 2D phase errors, which are both range and cross-range dependent. We propose a sparsity-driven method for joint SAR imaging and correction of 1D as well as 2D phase errors. This method performs phase error correction during the image formation process and provides focused, high-resolution images. Experimental results show the effectiveness of the approach.

**Index Terms**— Motion errors, phase errors, autofocus, regularization, synthetic aperture radar, sparsity

## 1. INTRODUCTION

In many imaging systems model errors are one of the important problem sources. This type of errors generally appears due to inaccurate measurement of the motion or position of the sensing platform or the observed object. Furthermore, various environmental effects result in similar type of errors. A well-known and widely-studied example of this type of errors appears in synthetic aperture radar (SAR) imaging. In SAR imaging, the time required for the transmitted signal to propagate to the field center and back may not be measured exactly. One of the reasons of this imperfection is the difficulty of determining the distance between the SAR platform and the field center extremely accurately. In addition, environmental effects such as atmospheric turbulence may induce random delays in the transmitted signal [1], which cause errors in the measured propagation time. These uncertainties appear as phase errors in the SAR data. The effects of phase errors are seen as defocusing (blurring) and loss of contrast in the reconstructed image [1]. Since in every aperture position a new signal is transmitted and the error for each signal is different, the most widely encountered phase errors are only in the cross-range direction, which means that the phase error is a function of the aperture position (cross range). However, in low frequency UWB SAR systems, severe propagation effects may appear through the ionosphere, including Faraday rotation, dispersion, and scintillation [2] which cause 2D phase errors, defocusing the reconstructed image in both range and cross-range directions. Moreover, in 3D SAR imaging, phase errors are both range and cross range dependent. To remove the phase errors many techniques have been devel-

oped which are called autofocus techniques. Most of them are based on post-processing of the conventionally reconstructed SAR image [3–7]. However, we know that conventional imaging does not perform well in sparse aperture scenarios or when the data are incomplete. On the other hand, regularization based image reconstruction has successfully been applied to SAR imaging and it is shown that it has many advantages over conventional imaging [8]. These techniques can alleviate the problems in the case of incomplete data or sparse aperture. Moreover, they produce images with increased resolution, reduced sidelobes, and reduced speckle by incorporation of prior information about the features of interest and imposing various constraints (e.g., sparsity, smoothness) about the scene. However, they assume that there are no uncertainties in the observation model. Motivated by these observations and considering that in SAR imaging, the underlying field has most of the time a sparse structure, we propose a sparsity-driven technique for joint SAR imaging and phase error correction by using a non-quadratic regularization based framework. We presented a limited version of this idea, only for 1D cross-range phase errors in [9]. The algorithm is an iterative algorithm, which is based on minimization of a cost function of both the field and the phase error. In the first step of every iteration, an estimate of the field is found and using the field estimate in the second step, phase error is estimated and compensated. Depending on the dimension and structure of the phase error, error estimation step is performed differently. We have implemented the proposed method for 2D separable and non-separable phase errors. Here we show results for SAR imaging but this idea can be implemented for other observation systems, in which similar types of errors occur.

## 2. SAR IMAGING

### 2.1. SAR Observation Model

SAR is generally used for imaging of the ground from a plane or satellite. On its flight path, a SAR sensor transmits pulses to the ground and then receives the reflected signals. In most SAR applications, chirp signals are transmitted. A chirp signal has the following form:

$$s(t) = \text{Re} \{ \exp[j(\omega_0 t + \alpha t^2)] \} \quad (1)$$

where  $\omega_0$  is the center frequency and  $2\alpha$  is the so-called chirp-rate. The received signal  $q_\theta(t)$  at a certain aperture position  $\theta$  involves the convolution of the transmitted chirp signal with the projection  $p_\theta(u)$  of the field at that observation angle.

$$q_\theta(t) = \text{Re} \left\{ \int p_\theta(u) \exp[j[\omega_0(t - \tau_0 - \tau(u)) + \alpha(t - \tau_0 - \tau(u))^2]] du \right\} \quad (2)$$

If we let the distance from the SAR platform to the center of the field be  $R$ ,  $\tau_0 + \tau(u)$  is the delay for the returned signal from the

---

This work was partially supported by the Scientific and Technological Research Council of Turkey under Grant 105E090, and by a Turkish Academy of Sciences Distinguished Young Scientist Award.

scatterer at the range position  $R + u$ . Here,  $\tau_0$  is the time required for the transmitted signal to propagate to the scene center and back. The data used for imaging are obtained after a pre-processing step. In particular, the returned signal is first multiplied with delayed in-phase and quadrature versions of the transmitted chirp signal and then the output is low-pass filtered. After this process, the relation between the field  $f(x, y)$  and the pre-processed SAR data  $r_\theta(t)$  becomes

$$r_\theta(t) = \iint_{x^2+y^2 \leq L^2} f(x, y) \exp\{-jU(x \cos \theta + y \sin \theta)\} dx dy \quad (3)$$

where

$$U = \frac{2}{c}(\omega_0 + 2\alpha(t - \tau_0)) \quad (4)$$

and  $L$  is the radius of the illuminated area. All of the returned signals from all observation angles constitute a patch from the two dimensional spatial Fourier transform of the corresponding field. The corresponding discrete model including all returned signals is as follows.

$$\underbrace{\begin{bmatrix} r_{\theta_1} \\ r_{\theta_2} \\ \vdots \\ r_{\theta_M} \end{bmatrix}}_r = \underbrace{\begin{bmatrix} C_{\theta_1} \\ C_{\theta_2} \\ \vdots \\ C_{\theta_M} \end{bmatrix}}_C f \quad (5)$$

where  $r_{\theta_m}$  is the vector of observed samples,  $C_{\theta_m}$  is discretized approximation to the continuous observation kernel at the observation angle  $\theta_m$  and  $f$  is a vector representing the unknown sampled reflectivity image. The data  $r$  are the phase histories. If we consider that there is also measurement noise, the observation model becomes

$$g = Cf + v \quad (6)$$

where  $v$  stands for measurement noise which is assumed to be white Gaussian noise and  $g$  is the noisy observation. Since the phase history data are two dimensional spatial Fourier transform of the field, conventional imaging (polar format algorithm) for SAR is based on the 2D inverse Fourier transform.

## 2.2. Phase Errors

Any error on  $\tau_0$  (defined in Section 2.1), causes phase errors in the SAR data. The delay in every aperture position is usually assumed to be constant, which means that phase error varies only in the cross-range direction. However, ionospheric effects on the transmitted signal, especially for low frequency UWB SAR systems cause 2D phase errors. Moreover, waveform errors such as frequency jitter from pulse to pulse, transmission line reflections and waveguide dispersion effects [10] may cause defocus in both range and cross-range direction. If there is a 2D phase error, it means that every sample point of the phase history data is perturbed with a different phase error. The relation between the erroneous and error-free data for every phase history sample can be expressed as

$$r_\epsilon(s) = e^{j\phi(s)} r(s) \quad (7)$$

where  $r(s)$  and  $\phi(s)$  denote  $s$ -th sample of the phase history data and the corresponding phase error, respectively. In terms of observation model, the same relationship can be expressed as

$$C_s(\phi(s))f = e^{j\phi(s)} C_s f \quad (8)$$

Here,  $C_s$  represents the part of the model matrix  $C$  for the  $s$ -th data sample.

## 3. SPARSITY-DRIVEN IMAGE RECONSTRUCTION

Regularization based image reconstruction techniques provide stable and reasonable estimates of the field  $f$  by incorporation of the prior knowledge about the field into the image formation process. These techniques formulate image formation as an optimization problem. The cost functional is composed of a least-squares data fidelity term, as well as a side constraint related to the features of interest. In particular, this side constraint incorporates information about the structure of the scene (sparsity, smoothness etc.) into the optimization problem. In many imaging problems, the field of interest admits a sparse representation in some domain. In particular, in the context of SAR imaging of man-made objects, the underlying scene, dominated by strong metallic scatterers, is sparse, i.e. there are few nonzero pixels. In such a case, a solution with great energy concentration is needed. To provide it, a non-quadratic side constraint is appropriate. There are a variety of non-quadratic choices to use as the side constraint. The general family of  $l_p$ -norms is one of them. In spectral analysis,  $l_p$ -norm constraints, where  $p < 2$ , have been shown to result in higher resolution spectral estimates compared to the  $l_2$ -norm case. Moreover, smaller value of  $p$  implies less penalty on large pixel values as compared to larger  $p$  [8]. Based on these observations,  $l_p$ -norm constraints with  $p < 2$  are good choices to obtain sparse solutions. Here we consider one of many specific cases. Image formation is performed solving the following optimization problem.

$$\hat{f} = \arg \min_f \|g - Cf\|_2^2 + \lambda \|f\|_p^p \quad (9)$$

The first term enforces data fidelity, whereas the second term enforces sparsity of the field. The scalar parameter  $\lambda$  is known as the regularization parameter which determines the relative weight of these two terms in the solution.

## 4. PROPOSED METHOD

We propose a sparsity-driven technique for joint SAR imaging and phase error correction. This technique is capable of handling 1D as well as 2D phase errors. We consider two cases of 2D phase errors as separable and non-separable. What we mean by ‘separable’ is that the 2D phase error is composed of a range varying and cross-range varying 1D phase error functions. In non-separable case the 2D phase error cannot be separated into two 1D error functions. The algorithm is an iterative algorithm, which cycles through steps of image formation and phase error estimation and compensation. It is based on the minimization of the following cost function, with respect to  $\phi$  and  $f$  using coordinate descent technique.

$$J(f, \phi) = \|g - C(\phi)f\|_2^2 + \lambda \|f\|_1 \quad (10)$$

In the first step of every iteration the cost function  $J(f, \phi)$  is minimized with respect to  $f$ . This is the image formation step and same for all type of phase errors.

$$\begin{aligned} \hat{f}^{(n+1)} &= \arg \min_f J(f, \phi^{(n)}) = \\ & \arg \min_f \left\| g - C(\phi^{(n)})f \right\|_2^2 + \lambda \|f\|_1 \end{aligned} \quad (11)$$

where  $n$  denotes the iteration number. Note that  $C(\phi^{(n)})$  denotes the model matrix corresponding to the phase error obtained in the

$n$ -th iteration. Second step is the phase error estimation step where a different procedure is implemented for different types of phase errors.

#### 4.1. 1D Phase Errors

If the phase error is a 1D cross-range varying phase error, given the field estimate, the following cost function is minimized for every aperture position [9]

$$\begin{aligned} \widehat{\Delta\phi}_m^{(n+1)} &= \arg \min_{\Delta\phi_m} J(\hat{f}^{(n+1)}, \Delta\phi_m) = \\ \arg \min_{\Delta\phi_m} &\left\| g_m - \exp(j\Delta\phi_m) C_m(\hat{\phi}_m^{(n)}) \hat{f}^{(n+1)} \right\|_2^2 \\ &\text{for } m = 1, 2, \dots, M \end{aligned} \quad (12)$$

where  $\widehat{\Delta\phi}_m^{(n+1)}$  denotes the incremental phase error estimate for the  $m$ -th aperture position in the iteration  $(n+1)$ . In (12),  $g_m$  and  $C_m(\phi_m)$  stand for the part belonging to the  $m$ -th aperture position of the SAR data and the model matrix, respectively. The optimization problem in (12) is solved in closed form for every aperture position. The solution of the problem in (12) results in the following expression

$$\widehat{\Delta\phi}_m^{(n+1)} = -\arctan\left(\frac{-I}{R}\right) \quad (13)$$

where

$$R = \text{Re}\{\hat{f}^H C_m(\hat{\phi}_m^{(n)})^H g_m\} \quad I = \text{Im}\{\hat{f}^H C_m(\hat{\phi}_m^{(n)})^H g_m\} \quad (14)$$

Using the incremental phase error estimate, the model matrix is updated as in (15) and the algorithm turns back to the image formation step of the next iteration.

$$C_m(\hat{\phi}_m^{(n+1)}) = \exp(j\widehat{\Delta\phi}_m^{(n+1)}) C_m(\hat{\phi}_m^{(n)}) \quad (15)$$

#### 4.2. 2D Separable Phase Errors

If the phase error is a 2D separable phase error then in the phase error estimation step of every iteration, first, the phase error estimate for cross-range is found as in (12). After updating the model matrix, the incremental phase error estimate for the range direction is found repeating the same procedure as in cross-range direction, this time for every range position. Then the model matrix is updated using the range dependent incremental phase error and the algorithm passes to the next iteration.

#### 4.3. 2D Non-separable Phase Errors

In a more general case in which we consider 2D non-separable phase errors, phase error estimation is done for every sample of the phase history data, since all sample points are perturbed with different and potentially independent phase errors. Therefore, using the same point of view as in the previous two cases, in the phase error estimation step, the following cost function is minimized.

$$\begin{aligned} \widehat{\Delta\phi}_s^{(n+1)} &= \arg \min_{\Delta\phi_s} J(\hat{f}^{(n+1)}, \Delta\phi_s) = \\ \arg \min_{\Delta\phi_s} &\left\| g_s - \exp(j\Delta\phi_s) C_s(\hat{\phi}_s^{(n)}) \hat{f}^{(n+1)} \right\|_2^2 \\ &\text{for } s = 1, 2, \dots, S \end{aligned} \quad (16)$$

where  $\widehat{\Delta\phi}_s^{(n+1)}$  denotes the incremental phase error estimate for the  $s$ -th element of the phase history data. Here  $g_s$  and  $C_s(\phi_s)$  stand for the  $s$ -th element of the SAR data and the corresponding row of the model matrix, respectively. This step is solved in closed form similar to that in (13). The solution of the optimization problem in (16) is as follows.

$$\widehat{\Delta\phi}_s^{(n+1)} = -\arctan\left(\frac{-I}{R}\right) \quad (17)$$

where

$$R = \text{Re}\{\hat{f}^H C_s(\hat{\phi}_s^{(n)})^H g_s\} \quad I = \text{Im}\{\hat{f}^H C_s(\hat{\phi}_s^{(n)})^H g_s\} \quad (18)$$

If we let the number of cross-range positions be  $M$  and the number of range positions be  $K$ , then we can say that in a 1D cross-range phase error case, we solve the problem for  $M$  unknowns, in a 2D separable phase error case for  $M+K$  unknowns, and in a 2D non-separable phase error case for  $M \times K$  unknowns. Hence, correcting for 2D non-separable phase errors is a much more difficult problem than the others.

## 5. EXPERIMENTAL RESULTS

We present results on two public SAR data sets provided by the U.S. Air Force Research Laboratory (AFRL): the ‘Slicy’ data, part of the MSTAR dataset [11]; and the ‘Backhoe’ data [12]. On Slicy data we have applied a 2D non-separable phase error which is uniformly distributed in  $[-\pi, +\pi)$ . In Figure 1(a) and (b) the conventional image and the image formed by sparsity-driven image reconstruction for the error-free case are presented, respectively. Figure 1(c) shows the conventional image reconstructed from data with phase errors, whereas Figure 1(d) shows the result of the proposed method. As seen from the figures, the proposed method provides the advantages of the sparsity-driven imaging while removing the defocus effect of the phase error effectively. Another dataset on which we present results is the Backhoe dataset. To deal with the wide-angle observations in the Backhoe dataset, we incorporate the subaperture-based composite imaging approach of [13] into our framework. The Backhoe dataset is perturbed with a 2D separable phase error which is composed of two 1D phase error functions. One of these error functions is only range dependent where the other is only cross-range dependent. These 1D errors are uniformly distributed in  $[-3\pi/4, +3\pi/4]$ . Figure 2(a) and (b) show the conventional image and the image reconstructed by sparsity-driven imaging, respectively, when there is no phase error. The conventional image and the result of the proposed method in the case of phase errors are shown in Figure 2(c) and (d), respectively. These results demonstrate the effectiveness of the proposed method.

## 6. CONCLUSION

In this study, we have proposed a sparsity-driven technique for joint SAR imaging and phase error correction. The method can handle 1D phase errors as well as 2D separable and non-separable phase errors. The method corrects the phase errors during the image formation process while it produces high resolution focused SAR images, thanks to its sparsity enforcing nature. Since the current formulation of the proposed method does not include any prior information of the phase error, especially for large phase errors it is possible to end up with focused but shifted images due to inherent ambiguities. To deal with this issue, the method can be extended incorporating some prior knowledge about the phase error or some region of support information about the scene.

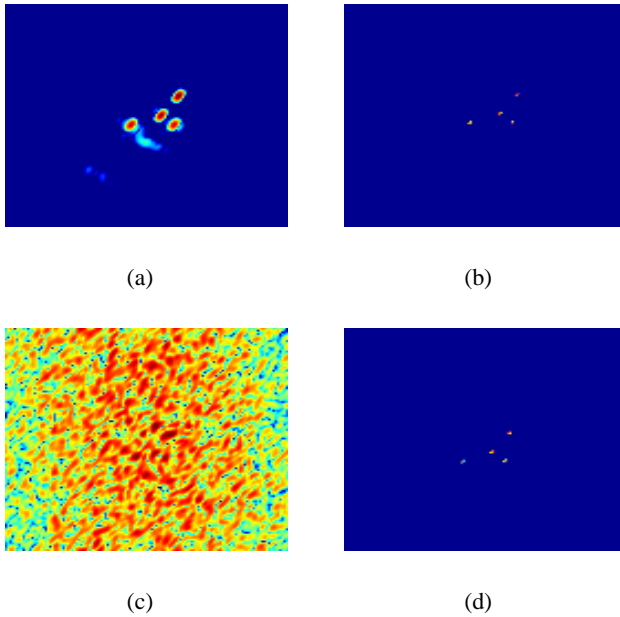


**Fig. 1.** a) Conventionally reconstructed image from data without phase errors b) Image reconstructed by sparsity-driven imaging from data without phase errors c) Conventionally reconstructed image from data corrupted by phase errors d) Image reconstructed by the proposed method from data corrupted by phase errors.

## 7. REFERENCES

- [1] C.V. Jakowatz, D.E. Wahl, P.H. Eichel, D.C. Ghiglia, and P.A. Thompson, *Spotlight-Mode Synthetic Aperture Radar: A Signal Processing Approach*, Springer, 1996.
- [2] D.W. Warner, D. Ghiglia, A. FitzGerrell, and J. Beaver, "Two-dimensional phase gradient autofocus," *Proc. SPIE*, vol. 4123, 2000.
- [3] D.E. Wahl, P.H. Eichel, D.C. Ghiglia, and C.V. Jakowatz, "Phase Gradient Autofocus - A robust tool for high resolution SAR phase correction," *IEEE Trans. Aerosp. Electron.Syst.*, vol. 30, no. 3, 1994.
- [4] C.E. Mancill and J.M. Swiger, "A map drift autofocus technique for correcting higher-order sar phase errors," *Proc. 27th Annual Tri-Service Radar Symp.*, 1981.
- [5] L. Xi, L. Guosui, and J. Ni, "Autofocusing of ISAR images based on entropy minimization," *IEEE Trans. Aerosp. Electron. Syst.*, vol. 35, no. 10, 1999.
- [6] F. Berizzi and G. Corsini, "Autofocusing of inverse synthetic aperture radar images using contrast optimization," *IEEE Trans. Aerosp. Electron. Syst.*, vol. 32, no. 7, 1996.
- [7] J.R. Fienup and J.J. Miller, "Aberration correction by maximizing generalized sharpness metrics," *J. Opt. Soc. Amer. A*, vol. 20, no. 4, 2003.
- [8] M. Çetin and W.C. Karl, "Feature-enhanced synthetic aperture radar image formation based on nonquadratic regularization," *IEEE Trans. Image Processing*, pp. 623–631, 2001.

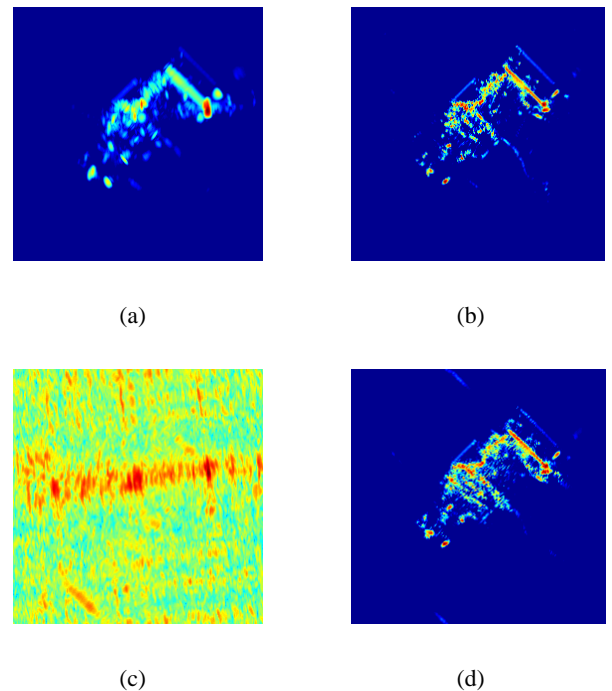


**Fig. 2.** a) Conventionally reconstructed image from data without phase errors b) Image reconstructed by sparsity-driven imaging from data without phase errors c) Conventionally reconstructed image from data corrupted by phase errors d) Image reconstructed by the proposed method from data corrupted by phase errors.

- [9] N.Ö. Önhon and M. Çetin, "A non-quadratic regularization based technique for joint SAR imaging and model error correction," *Proc. SPIE*, vol. 7337, 2009.
- [10] W.G. Carrara, R.M. Majewski, and R.S. Goodman, *Spotlight Synthetic Aperture Radar: Signal Processing Algorithms*, Artech House, 1995.
- [11] *MSTAR, Air Force Research Laboratory, Model Based Vision Laboratory, Sensor Data Management System*, <http://www.mbvlab.wpafb.af.mil/public/sdms/datasets/mstar/>.
- [12] *Backhoe Data Sample & Visual-D Challenge Problem, Air Force Research Laboratory, Sensor Data Management System*, <https://www.sdms.afrl.af.mil/main.htm>.
- [13] M. Çetin and R. L. Moses, "SAR imaging from partial-aperture data with frequency-band omissions," *Proc. SPIE*, vol. 5808, 2005.